Korean J. Chem. Eng., 35(3), 734-743 (2018)
DOI: 10.1007/s11814-017-0353-1

pISSN: 0256-1115
eISSN: 1975-7220

Evaluating isotherm models for the prediction of flue gas adsorption equilibrium and dynamics

Rai Hyoung Kang, Jehun Park, Dohyung Kang, and Jae W. Lee†

Department of Chemical and Biomolecular Engineering, Korea Advanced Institute of Science and Technology (KAIST), 291 Daehak-ro, Yuseong-gu, Daejeon 34141, Korea
(*Received 28 August 2017 • accepted 26 December 2017*)

Abstract−We evaluated isotherm models for the precise prediction of adsorption equilibrium and breakthrough dynamics. Adsorption experiments were performed using pure N_2, CO_2 and their binary mixture with an activated carbon (AC) material as an adsorbent. Both BET and breakthrough measurements were conducted at various conditions of temperature and pressure. The corresponding uptake amount of pure component adsorption was experimentally determined, and parameters of the four different isotherm models, Langmuir, Langmuir-Freundlich, Sips, and Toth, were calculated from the experimental data. The predictive capability of each isotherm model was also evaluated with the binary experimental results of binary N_2/CO_2 mixtures, by means of sum of square errors (SSE). As a result, the Toth model was the most precise isotherm model in describing CO_2 adsorption equilibrium on the AC. Based on the breakthrough experimental result from the binary mixture adsorption, non-isothermal modeling for the adsorption bed was performed. The breakthrough results with all of the isotherm models were examined by rigorous dynamic simulations, and the Toth model was also the most accurate model for describing the dynamics.

Keywords: CO_2 Adsorption, Isotherm, Breakthrough, Activated Carbon, Toth Model

INTRODUCTION

Although CO_2 has a minor global warming potential compared with other greenhouse gases such as methane (CH_4) or chlorofluorocarbons (CFCs), its tremendous emission amounts make it one of the major greenhouse gases (GHGs). It has the largest effect (82.4%) on global warming [1]. There have been numerous efforts for reducing CO_2 emissions [2]. The corresponding process is carbon capture and sequestration (CCS), which describes a comprehensive process for capture, transport, storage and utilization of CO_2.

To widen the application of the CCS process, several capturing methods have been proposed, such as liquid CO_2 absorption technique [3-5], or CO_2 capture in a solid hydrate form [6-8]. Another active area in CCS focuses on the CO_2 adsorption process using a porous solid adsorbent like zeolite, metallic organic frameworks (MOFs), and activated carbon (AC) [9,10]. Especially, in the case of CO_2 adsorption process using a solid adsorbent, pressure or temperature swing adsorption (PSA) process is the representative process and the corresponding field is seen as an ongoing research [9-11].

The goal of the breakthrough adsorption experiment using a fixed bed is to establish parameters of a mathematical dynamic model including mass transfer and isotherm equilibrium. Previous studies focusing on the isotherm model mainly adopted the Langmuir model to describe the gas-solid adsorption equilibrium system. After that, various isotherm models were introduced to determine the adsorbed amount of gas more precisely. Both Toth isotherm and Dubinin-Astakhov isotherm models were exploited for CO_2 adsorption modeling on AC [12]. The adsorption equilibrium of CO_2, CH_4, and N_2 mixture was explained in the breakthrough experiment by utilizing the Sips isotherm model [13]. The parameters of the multisite-Langmuir isotherm model [14] were determined using experimental data of various gases. Rufford et al. utilized and compared four isotherm models of Langmuir, Langmuir-Freundlich, Sips and Toth isotherm to describe binary gas adsorption equilibrium [15].

Modeling a mass transfer coefficient (MTC, k_i) also played an essential role in the adsorption kinetic work, and similar to the equilibrium isotherm study, various kinetic models were introduced. Rashidi et al. analyzed CO_2 adsorption kinetics with four different kinetics models via time-dependent mass analyzing method [16]. Dantas et al. used the linear driving force (LDF) model to analyze the breakthrough dynamics and predicted the MTC of CO_2 on Zeolite 13X [17]. For the MTC model itself, some prior studies considered molecular diffusion at solid pores [18,19] and proposed the pressure-adaptive MTC model to explain CO_2 adsorption on a porous material [20].

Based on the H_2/CO_2 mixture gas adsorption experiment, Casas et al. performed kinetic modeling by using isotherm and mass transfer coefficient in the LDF model [21]. They showed a potential to apply the corresponding models for deriving PSA design sequences [22,23]. For the precise prediction of breakthrough adsorption dynamics, it is important to derive a more precise mass transfer and isotherm model. Apart from the simple comparison of the accuracy of isotherm models using adsorption equilibrium data, there has been no study related to screening proper isotherm

†To whom correspondence should be addressed.
E-mail: jaewlee@kaist.ac.kr, jaelee43@gmail.com

models in adsorption dynamic models. Rufford et al. used various isotherm models for the prediction of adsorption equilibrium [15], but they used the Langmuir model alone for predicting the adsorption breakthrough dynamics.

Hence, we first evaluated various isotherm models for the precise prediction of breakthrough adsorption dynamics. Langmuir, Langmuir-Freundlich, Sips, Toth and their extended models were chosen for comparison, and the deviations between experimental results from fixed-bed breakthrough and calculation results from the isotherm models were determined. It was confirmed that the isotherm model estimated from pure component adsorption data can be extended to the binary gas adsorption. Even if prior works mostly focused on the adsorption equilibrium, we investigated the suitability of adsorption isotherm model as a part of adsorption kinetics model at the transient region. Finally, a general mass transfer model was proposed by analyzing the breakthrough experiments with the most accurate isotherm model.

MODELING

1. Assumption

To simulate the dynamics of gas adsorption in a fixed bed, mathematical modeling of material and energy balance was carried out with the following assumptions: 1) the radial gradient of temperature and concentration was ignored, 2) the ambient temperature surrounding the fixed bed was constantly maintained, 3) the structural properties of the fixed bed such as porosity and adsorbent shape remained unchanged during the adsorption process, and 4) gas flows only along the axial direction.

2. Material and Momentum Balance

The adsorption process using a solid adsorbent is considered as a 1-D process in a fixed-bed. The radial dispersion is neglected because of a small diameter compared to the length. The material balance [20] for each gas component can be formulated as,

$$\frac{\partial(u_g c_i)}{\partial z}+\varepsilon_b\frac{\partial c_i}{\partial t}+J_i=0 \tag{1}$$

where u_g is a velocity of gas, z is the distance from the bed inlet, c_i is a concentration of component i, ε_b is the overall porosity of the bed, and J_i is the mass transfer rate of component i. The mass transfer rate describes the mass transfer between solid adsorbent and gaseous phase and can be expressed as,

$$J_i=\rho_s\frac{\partial q_i}{\partial t}=\rho_s k_i(q_i^*-q_i) \tag{2}$$

where ρ_s is a solid bulk density, k_i is a mass transfer coefficient which is a constant or variable in this study, q_i^* is the adsorption amount at equilibrium that will be described by an isotherm model, respectively. Here, the mass transfer rate is expressed in form of the linear driving force (LDF) model. The mass transfer coefficient used in the LDF model is obtained from dynamic breakthrough simulations performed based on different isotherm models by using ASPEN Adsorption™, which will be discussed later. The momentum balance equation is estimated by Ergun equation considering the pressure gradient caused by pressure drop inside of the fixed-bed [24].

$$\frac{dp}{dz}=150\frac{\mu u_g(1-\varepsilon_b)^2}{D_p^2\,\varepsilon_b^3}+1.75\frac{\rho_g u_g 1-\varepsilon_b}{D_p\,\varepsilon_b^3} \tag{3}$$

where D_p is the diameter of packed adsorbent and μ is the gas viscosity, respectively.

3. Energy Balance

Since adsorption is exothermic and it is a temperature-sensitive process, non-isothermal adsorption modeling is required. Conductive heat transfer along the axial and radial directions can be neglected because convective heat transfer is much more dominant than conductive heat transfer in both gas and solid phases. Considering the heat transfer between solid, gas and wall phases, the energy balance [20] can be written in two different equations:

$$\rho_s C_{ps}\frac{\partial T_s}{\partial t}+\rho_s\Sigma_i\left(\Delta H_i\frac{\partial q_i}{\partial t}\right)+C_{vg}u_g\rho_g\frac{\partial T_g}{\partial t}+P\frac{\partial u_g}{\partial t}+\frac{4H_I}{D_I}(T_g-T_w)=0 \tag{4}$$

where C_{ps} is a specific heat capacity of solid adsorbent, T_s is the adsorbent temperature, ΔH_i is a heat of adsorption of component i, C_{vg} is a specific heat capacity of gas, P is pressure, H_I is a heat transfer coefficient between gas and wall, T_w is the wall temperature, and D_I is an inner diameter of column, respectively. Energy balance around the bed wall is formulated as,

$$-k_w\frac{\partial^2 T_w}{\partial z^2}+\rho_w C_{pw}\frac{\partial T_w}{\partial t}-H_I\frac{4D_I^2}{D_O^2-D_I^2}(T_g-T_w)+H_O\frac{4D_O^2}{D_O^2-D_I^2}(T_w-T_{amb})=0 \tag{5}$$

where k_w is a wall thermal conductivity, D_O is an outer diameter of column, H_O is a thermal conductivity between wall and ambient, T_{amb} is the ambient temperature, respectively. Here, the distinction from the first solid-gas phase energy balance is the thermal dissipation on the wall.

EXPERIMENTAL SECTION

1. Instrument and Material

In this study, AC material (Norit RB3, Sigma-Aldrich) was used as a solid adsorbent for the adsorption of pure and binary mixture gas of N_2 and CO_2. In this step, a sphere-shaped adsorbent pellet with a diameter of 3 mm was packed in the column. The adsorbent was surrounded by 2 mm diameter glass beads and quarts wool to avoid the adsorbent being scattered. The adsorbent properties such as particle diameter, density, amount, porosity are listed in Table 1 with the column dimension. The gases utilized in this study are N_2 (Air Liquide Korea, 99.999%), CO_2 (Air Liquide Korea, 99.5%), and He (Air Liquide Korea, 99.999%).

The BET analyzer, three-flex surface characterization analyzer (Micromeritics, USA) was employed for analyzing and measuring the adsorption equilibria at the low pressure condition. A lab-made fixed-bed in Fig. 1 was used for measuring equilibrium adsorption amounts above 1.5 bars through breakthrough experiments. A mass flow controller (MFC) was installed to control the mass flow of N_2 and CO_2 from the gas canister. One back-pressure regulator was installed for controlling gas pressure, and the other back-

Table 1. Dimensions of the adsorption bed

Index	Value	Units
Inner diameter (D_I)	0.01092	m
Outer diameter (D_O)	0.0127	m
Column length	0.3	m
Total length of glass bead packing section	0.047	m
Bed length (L)	0.253	m
Bed volume (V_b)	2.37×10^{-5}	m^3
Bed weight (w_b)	0.011378	kg
Bed density (ρ_b)	480.1868	kg/m^3
Bed porosity (ε_b)	0.395	-
Particle radius (r_p)	1.5×10^{-3}	m
Particle density (ρ_p)[14]	795	kg/m^3
Wall density (ρ_w)	7800	kg/m^3
Specific heat capacity of solid (C_{ps})	1050	J/kg·K
Specific heat capacity of wall (C_{pw})[19]	960	J/kg·K
Gas-Wall heat transfer coefficient (H_I)	66	$W/m^2\cdot K$
Wall-Ambient heat transfer coefficient (H_O)	700	$W/m^2\cdot K$
Solid thermal conductivity (k_s)	0.5	W/m·K
Gas thermal conductivity (k_g)*	0.025	W/m·K
Wall thermal conductivity (k_w)	16.2	W/m·K

*The value of k_g is calculated by ASPEN Plus 8.8™

pressure regulator at the downstream of the bed was for controlling the sorption pressure of the fixed bed. An experimental temperature was set and maintained constant by a water bath. The thermocouple inserted in the fixed bed monitored temperature changes in the bed. The composition of outlet gas was monitored by the mass spectrometer, MS (Pfeiffer Vacuum, Switzerland).

2. Dynamic Breakthrough Experiment

Before each breakthrough measurement, the fixed-bed packed with the adsorbent was heated to 150 °C for desorption of any left-over gas. Once the internal bed reached a specific temperature, the bed was evacuated down to 0.01 bar by a vacuum pump. After that, the experimental pressure condition was managed by He gas at a volumetric flowrate of 20 sccm. The adsorbate gas was provided by manipulating MFC and BPR. When both pressure and flow were stabilized, both valves of upstream and downstream of the bed were opened while simultaneously blocking the flow of He. In case of pure gas adsorption, each N_2 or CO_2 gas was injected into the fixed bed while maintaining experimental temperature (30 °C, 50 °C and 70 °C) and pressure (1.5, 3 and 5 bars) at a flowrate of 120 sccm (0.098 mmol·s^{-1}) N_2 or 40 sccm (0.028 mmol·s^{-1}) CO_2. In the case of a gas mixture of N_2/CO_2 with a molar ratio of 2 : 1, the binary gas was injected with 80 sccm (0.063 mmol·s^{-1}) N_2 and 40 sccm (0.028 mmol·s^{-1}) CO_2. Similarly, another mixture of 4 : 1 was provided with 160 sccm (0.13 mmol·s^{-1}) N_2 and 40 sccm (0.028 mmol·s^{-1}) CO_2.

The dynamic breakthrough curves of outlet gas were obtained by a mass spectrometer. Referring to Becnel et al., the equilibrium amount of the adsorption was determined by analyzing the dynamic breakthrough data in the following equations [25]:

$$t_t\,(\text{sec}) = \int_0^{\infty}\left(1-\frac{c_i(\tau)}{c_{i0}}\right)d\tau \tag{6}$$

where t_t is a saturation time, $c_i(\tau)$ is a molar concentration of component i monitored by the mass spectrometer at time τ, and c_{i0} is an initial molar concentration of component i. Therefore, the total amount of adsorption is given as,

$$q_i^*\,(\text{mol/kg}) = \frac{1}{w_b}\left(F\cdot y_i\cdot\int_0^{t_t}\left(1-\frac{c_i(\tau)}{c_{i0}}\right)d\tau\right)-\frac{\varepsilon_b c_{ib}}{\rho_b} \tag{7}$$

where q_i^* is the adsorption amount of component i at equilibrium, F is a total molar flowrate, y_i is a mole fraction of component i, ε_b is the bed porosity, c_{ib} is a molar concentration of component i and ρ_b is the bed density, respectively. The last term of the equation above describes the amount of gas that exists in the adsorbent pore without physical adsorption during the dynamic breakthrough experiment. Also, the bed porosity, ε_b, can be obtained from the following equation:

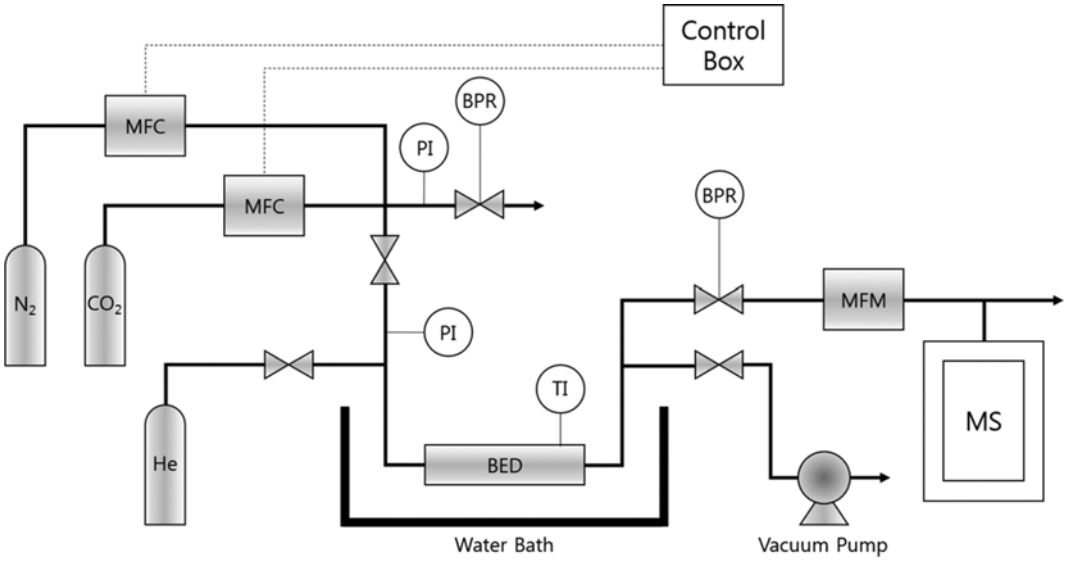

Fig. 1. Dynamic breakthrough experimental apparatus.

$$\varepsilon_b = \varepsilon_i + (1-\varepsilon_i)\varepsilon_p \quad (8)$$

where ε_i is the inter-particle porosity and ε_p is the intra-particle porosity.

3. Isotherm Model and Parameter Estimation

To determine the isotherm model that most precisely describes the experimental result, the parameters for four different isotherm models (Langmuir, Langmuir-Freundlich, Sips and Toth) were estimated from pure component adsorption experiments. For the binary mixture adsorption, their extended models were introduced. In this study, the parameters of each isotherm model, K_i and q_i are expressed by the Arrhenius term for describing the temperature dependency as follows:

for Langmuir (Eq. (9-1))/Extended Langmuir (Eq. (9-2))

$$q_i^{Lang} = q_{i,max}^{Lang}\frac{K_i p_i}{1+K_i p_i} \quad (9\text{-}1)$$

$$q_i^{Lang} = q_{i,max}^{Lang}\frac{K_i p_i}{1+\Sigma_j^m (K_j p_j)} \quad (9\text{-}2)$$

$$K_i = K_{i,0}\exp\left(-\frac{\theta_{Lang}}{RT}\right) \quad (9\text{-}3)$$

for Langmuir-Freundlich (Eq. (10-1))/Extended Langmuir-Freundlich (Eq. (10-2))

$$q_i^{LF} = q_{si}^{LF}\frac{K_i p_i^n}{1+K_i p_i^n} \quad (10\text{-}1)$$

$$q_i^{LF} = q_{si}^{LF}\frac{K_i p_i^n}{1+\Sigma_j^m (K_j p_j^n)} \quad (10\text{-}2)$$

$$K_i = K_{i,0}\exp\left(-\frac{\theta_{LF}}{RT}\right) \quad (10\text{-}3)$$

$$q_{si}^{LF} = q_{i,0}^{LF}\exp\left(-\frac{\Theta_{LF}}{RT}\right) \quad (10\text{-}4)$$

for Sips (Eq. (11-1))/Extended Sips (Eq. (11-2))

$$q_i^{S} = q_{si}^{S}\frac{(K_i p_i)^n}{1+(K_i p_i)^n} \quad (11\text{-}1)$$

$$q_i^{S} = q_{si}^{S}\frac{(K_i p_i)^n}{1+\Sigma_j^m (K_j p_j)^n} \quad (11\text{-}2)$$

$$K_i = K_{i,0}\exp\left(-\frac{\theta_S}{RT}\right) \quad (11\text{-}3)$$

$$q_{si}^{S} = q_{i,0}^{S}\exp\left(-\frac{\Theta_S}{RT}\right) \quad (11\text{-}4)$$

and for Toth (Eq. (12))

$$q_i^{T} = q_{i,0}^{T}\frac{K_i p_i}{(1+(K_i p_i)^n)^{1/n}} \quad (12\text{-}1)$$

$$K_i = K_{i,0}\exp\left(-\frac{\theta_T}{RT}\right) \quad (12\text{-}2)$$

Based on the experimental result of pure adsorption data, parameter estimation of the four isotherm models was conducted. In this estimation procedure, the objective function was established for the precise fitting of each isotherm with the experimental result. The least square method was chosen for the objective function (SSE: sum of square errors) as follows:

$$SSE = \Sigma_{p=1}^{3}\Sigma_{T=1}^{3}\Sigma_{k=1}^{n}(q_{exp,k,T,p} - q_{calc,k,T,p})^2 \quad (13)$$

where p is the case number of the pressure condition, T is the case number of the temperature condition and k is the case number of measured points by BET and breakthrough experiments. To obtain the parameters, the optimization runs were conducted by the non-linear GRG (Generalized reduced gradient) method.

RESULTS AND DISCUSSION

1. Pure Adsorption Equilibria Measurement

Adsorption amounts of pure CO_2 and N_2 from the breakthrough experiment at 1.5, 3, and 5 bars and at 30 °C, 50 °C and 70 °C are shown in Tables 2 and 3. The adsorbed amount of each gas was also measured by BET at a pressure range of 0 to 1.2 bar. Fig. 2 shows that there was not much deviation between the adsorbed gas amount measured by the fixed bed experiment and that measured by BET when extrapolating the BET data. The detailed adsorption amount measured from the BET apparatus and the breakthrough of the fixed-bed are included in Supporting

Table 2. Adsorption amount of pure CO_2 on activated carbon

Pressure (bar)[a]	Temperature (°C)[b]	Amount of adsorbed CO_2 ($mol \cdot kg^{-1}$)
1.5	30	1.81006
	50	1.31151
	70	0.94983
3	30	2.88001
	50	2.17774
	70	1.63883
5	30	3.93426
	50	2.98238
	70	2.36521

[a]Pressure uncertainty, u(p): 1 kPa
[b]Temperature uncertainty, u(T): 0.1 °C

Table 3. Adsorption amount of pure N_2 on activated carbon

Pressure (bar)[a]	Temperature (°C)[b]	Amount of adsorbed N_2 ($mol \cdot kg^{-1}$)
1.5	30	0.29292
	50	0.20232
	70	0.16736
3	30	0.61733
	50	0.49389
	70	0.38844
5	30	1.00295
	50	0.82144
	70	0.67418

[a]Pressure uncertainty, u(p): 1 kPa
[b]Temperature uncertainty, u(T): 0.1 °C

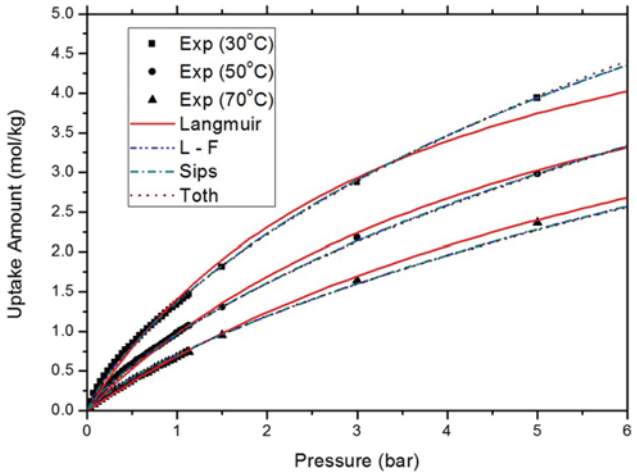

Fig. 2. Pure CO_2 adsorption equilibria. Predicted isotherm model with simulation results.

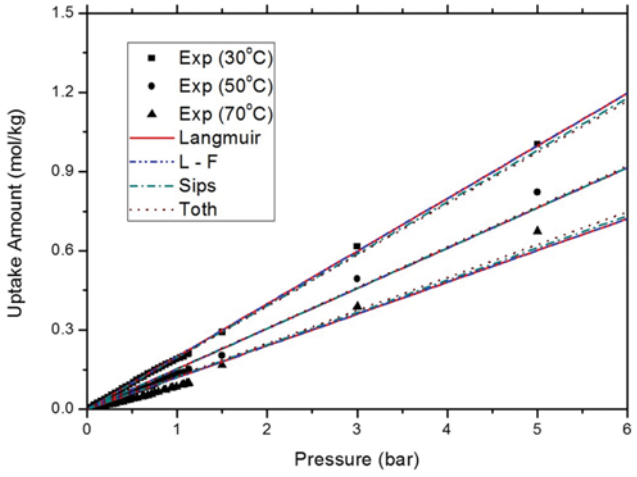

Fig. 3. Pure N_2 adsorption equilibria. Predicted isotherm model with simulation results.

Information (Tables S1 and S2).

With experimental data obtained, the parameters of each isotherm for the pure component adsorption were determined and plotted as in Figs. 2 and 3. All of the parameters are listed in Table 4. By comparing the value of SSE, the order of precision of the isotherm with the estimated parameters is L-F>Sips>Toth>Langmuir for pure CO_2 adsorption, and Langmuir>L-F>Sips>Toth for pure N_2 adsorption. For the CO_2 case, the SSE values are significantly different from each other, i.e., SSE=0.06775 for L-F that is the most accurate isotherm and SSE for the least accurate Langmuir is 0.26991. This result may come from the unique feature of the isotherm models. According to Ho et al., the L-F isotherm and the Sips isotherm models can be reduced into Freundlich isotherm model at the low adsorbate concentration level as in Eqs. (10-1), (10-2), (11-1), and (11-2) [26]. Thus, both L-F and Sips models can effectively describe the BET experimental data rather than the Langmuir and Toth isotherm models.

However, for N_2, the highest and the lowest SSE values are not that different, 0.0393 for Toth and 0.0369 for Langmuir. Thus, all

Table 4. Estimated parameters for each isotherm

Isotherm	Parameter	CO_2	N_2	Unit
Langmuir isotherm	$q_{i,max}^{Lang}$	6.38288	1454.35	$mol \cdot kg^{-1}$
	$k_{i,0}$	0.00018	1.782×10^{-6}	bar^{-1}
	θ_{Lang}	18.5155	10.9489	$kJ \cdot mol^{-1}$
	SSE	0.26991	0.0369	$(mol \cdot kg^{-1})^2$
	ARE[a]	9.1277	23.6258	%
Langmuir-Freundlich isotherm	$q_{i,0}^{LF}$	12.5733	21.589	$mol \cdot kg^{-1}$
	Θ_{LF}	4.36×10^{-5}	10.9492	$kJ \cdot mol^{-1}$
	$k_{i,0}$	0.00024	0.00012	bar^{-1}
	θ_{LF}	15.6357	6.973×10^{-7}	$kJ \cdot mol^{-1}$
	N	0.81732	1	-
	SSE	0.06775	0.03692	$(mol \cdot kg^{-1})^2$
	ARE	5.1872	23.6265	%
Sips isotherm	$q_{i,0}^{S}$	12.5621	352.6351	$mol \cdot kg^{-1}$
	Θ_S	3.583×10^{-7}	10.2496	$kJ \cdot mol^{-1}$
	$k_{i,0}$	3.889×10^{-5}	9.535×10^{-6}	bar^{-1}
	θ_S	19.1238	1.0×10^{-5}	$kJ \cdot mol^{-1}$
	N	0.81749	1	-
	SSE	0.06776	0.03755	$(mol \cdot kg^{-1})^2$
	ARE	5.1906	24.1742	%
Toth isotherm	$q_{i,0}^{T}$	55.3633	834.2235	$mol \cdot kg^{-1}$
	$k_{i,0}$	3.379×10^{-5}	5.105×10^{-6}	bar^{-1}
	θ_T	19.0493	9.63522	$kJ \cdot mol^{-1}$
	N	0.34321	1.00027	-
	SSE	0.0724	0.0392	$(mol \cdot kg^{-1})^2$
	ARE	5.0068	25.4636	%

[a]Absolute relative error

of the isotherm models except for the SSE of Langmuir isotherm of CO_2 adsorption in Table 4 showed a relatively small deviation from the experimental results. This indicates that the estimation of the isotherm parameters is quite adequate as in Fig. 2 and confirms that there is no significant difference in the results from both BET and breakthrough experiments, as proved in the previous study [15].

2. Binary Mixture Component Adsorption

Based on the isotherm parameters estimated from the pure component adsorption, the equilibrium of binary mixture adsorption was evaluated. The equilibrium amount of the binary component adsorption was measured with gas mixtures of 2 : 1 and 4 : 1 N_2/CO_2. Thus, the partial pressure of each N_2 and CO_2 was different from the pure adsorption case and varied with the total pressure change. The adsorption amounts for all cases are listed in Tables 5 and 6. Figs. 4 and 5 show both the experimental results for the adsorbed amount of CO_2 and the predicted adsorption amounts from the isotherm model whose parameters were estimated from the pure component adsorption. The CO_2 adsorption capacity can be confirmed by the adsorbed amount depending on the CO_2 partial pressure condition with the pure component and the gas mixtures of 2 : 1 and 4 : 1 N_2/CO_2. When comparing between the cases of 4 : 1 mixture at 5 bars (p_{CO_2}=1 bar) and 2 : 1 mixture at

Table 5. Adsorption amount of CO_2 on activated carbon using 2 : 1 N_2/CO_2 mixture

P_{tot} (bar)[a]	Temperature (°C)[b]	Amount of adsorbed CO_2 ($mol \cdot kg^{-1}$)
1.5	30	0.814574
	50	0.601797
	70	0.421933
3	30	1.302507
	50	0.961581
	70	0.677307
5	30	1.840285
	50	1.348587
	70	1.026697

[a]Pressure uncertainty, u(p): 1 kPa
[b]Temperature uncertainty, u(T): 0.1 °C

Table 6. Adsorption amount of CO_2 on activated carbon using 4 : 1 N_2/CO_2 mixture

P_{tot} (bar)[a]	Temperature (°C)[b]	Amount of adsorbed CO_2 ($mol \cdot kg^{-1}$)
1.5	30	0.611094
	50	0.393887
	70	0.275114
3	30	0.977996
	50	0.650731
	70	0.447514
5	30	1.260893
	50	0.957963
	70	0.644048

[a]Pressure uncertainty, u(p): 1 kPa
[b]Temperature uncertainty, u(T): 0.1 °C

3 bars (p_{CO_2}=1 bar), almost the same amount of CO_2 is adsorbed on AC. Also, a similar result was obtained by comparing between pure component adsorption at 1.5 bars and 2 : 1 mixture at 5 bars (p_{CO_2}=1.67 bar). The parameters estimated from the experiment of the pure component adsorption were valid for the prediction of binary gas adsorption in the given range of temperature and pressure.

The SSEs of all measured points are given in Table 7. The prediction accuracy for each isotherm was in the order of Toth>L-F> Sips>Extended-Sips>Extended L-F>Langmuir>Extended Langmuir. However, the SSE values of the single component isotherm models are not much deviated from their extended models. Thus, in the extended isotherm models (m>1 in Eqs. (9)-(11)), the contribution factor of N_2 in the denominator adsorption term could be negligible compared with the nominator adsorption term, as reported in a previous work [17].

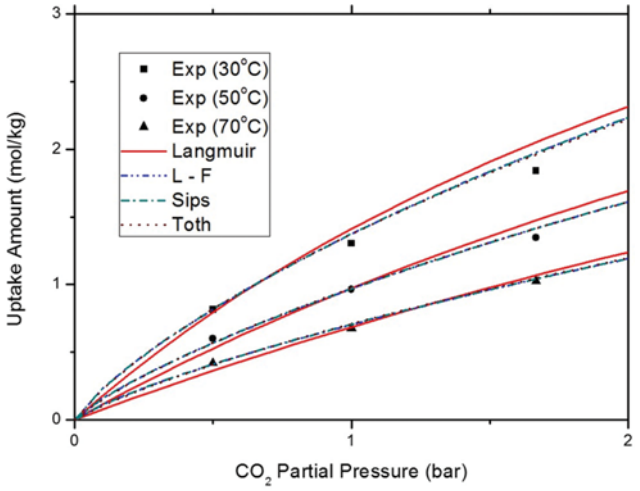

Fig. 4. Amount of CO_2 adsorption with 2 : 1 mixture at three different temperatures: experimental data and predicted isotherm models obtained by using pure component adsorption data.

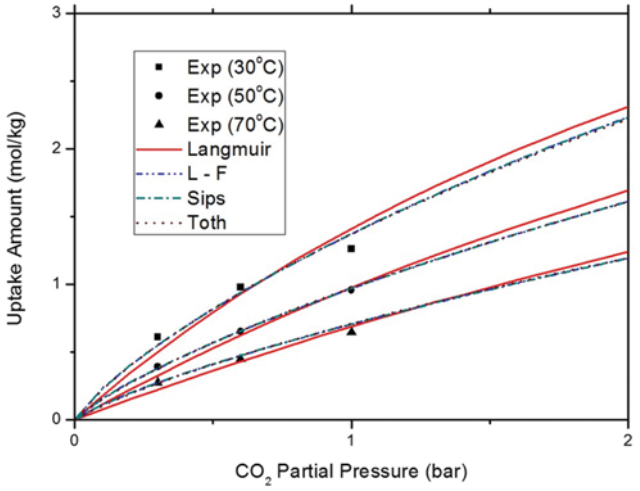

Fig. 5. Amount of CO_2 adsorption with 4 : 1 mixture at three different temperatures: experimental data and predicted isotherm models obtained by using pure component adsorption data.

3. Mass Transfer Coefficient Estimation

To design a CO_2 capture process using a solid adsorbent, the determination of mass transfer coefficient (MTC), k_i is essential for understanding the dynamics of adsorption bed. A constant MTC was estimated by using pure component adsorption data, and it was applied for the simulation of binary component adsorption processes [15]. In this study, however, the values for MTC were calculated from the binary N_2/CO_2 mixture adsorption experiment.

Accuracy of each isotherm model in the breakthrough dynamics was evaluated in two aspects: one error closely related to the adsorbed amount at equilibrium was derived from the prediction

Table 7. Predictive power of each isotherm model for mixture gas adsorption

Isotherm	Langmuir	Extended-Langmuir	L-F	Extended-L-F	Sips	Extended-Sips	Toth
SSE	0.1302	0.12961	0.05096	0.05051	0.05099	0.05099	0.04904

of the total CO_2 adsorption amount, and the other error from the transient region of the breakthrough curve is related to the MTC prediction in the adsorption kinetics. To deal with these, we set the following objective function (SSE) and find the values of k_i and Δt_j which minimize the objective function for every case of experiment [27].

$$SSE = \Sigma_{j=1}^{N} (c(t_j + \Delta t) - \hat{c}_j)^2 \quad (15)$$

where N is the number of measurements, $c(t_j)$ is the calculated outlet composition at a specific time, t_j, Δt is the time delay for the compensation of equilibrium error of each isotherm and $\hat{c}_j$ is the measured outlet composition at t_j.

Differing from a general parameter fitting procedure, the objective function introduced the time gap (Δt) to compensate for the predictive error of the equilibrium adsorption amount of the isotherm model in the dynamic breakthrough experimental data (Eq. (7)). Therefore, the SSE in Eq. (15) is an error occurring by the prediction of adsorption dynamics at the transient region.

Table 8. Mass transfer coefficient for 2 : 1 mixture derived from minimization of SSE

Condition		Mass transfer coefficient (1/s)			
Temperature	Pressure	Langmuir	L-F	Sips	Toth
30	1.5	0.1125	0.0572	0.0586	0.0621
	3	0.0645	0.0405	0.0413	0.0412
	5	0.0357	0.0294	0.0298	0.0290
50	1.5	0.1437	0.0708	0.0735	0.0822
	3	0.0571	0.0346	0.0352	0.0363
	5	0.0700	0.0417	0.0427	0.0425
70	1.5	0.3524	0.1276	0.1323	0.1618
	3	0.3175	0.0940	0.1023	0.1141
	5	0.1280	0.0577	0.0605	0.0627
$\sqrt{\Sigma(\Delta t)^2}$		95.97	44.29	41.41	37.75
SSE		0.0417	0.0940	0.0994	0.0815

Table 9. Mass transfer coefficient for 4 : 1 mixture derived from minimization of SSE

Condition		Mass transfer coefficient (1/s)			
Temperature	Pressure	Langmuir	L-F	Sips	Toth
30	1.5	0.0538	0.0400	0.0404	0.0439
	3	0.0491	0.0306	0.0308	0.0318
	5	0.0409	0.0282	0.0283	0.0282
50	1.5	0.1100	0.0664	0.0670	0.0766
	3	0.1077	0.0519	0.0532	0.0581
	5	0.0540	0.0331	0.0335	0.0345
70	1.5	0.3532	0.1380	0.1424	0.1781
	3	0.3226	0.1504	0.1614	0.1657
	5	0.1680	0.0695	0.0713	0.0785
$\sqrt{\Sigma(\Delta t)^2}$		90.72	59.10	59.43	58.60
SSE		0.0110	0.0187	0.0196	0.0135

One of the important parts of adsorption process modeling is to obtain the expression of overall MTC, k_i. The LDF model was utilized for the dynamic adsorption process in Eq. (16).

$$\frac{dq_i}{dt} = k_i(q_i^* - q_i) \quad (16)$$

The k_i values from the result of each simulation model with different gas compositions, temperature and pressure are listed in Tables 8 and 9. Figs. 6 and 7 are experimental breakthrough curves with simulation results of Langmuir and Toth isotherm models at different temperatures and pressures. The fitted constant value of k_i from the simulation describes the experimental result properly.

Considering k_i obtained from each isotherm in Tables 8 and 9, the Langmuir isotherm shows smaller SSE than the other models. As a result, Langmuir (SSE=0.0527) is the most descriptive adsorption model for the transient behavior, followed by Toth (SSE=

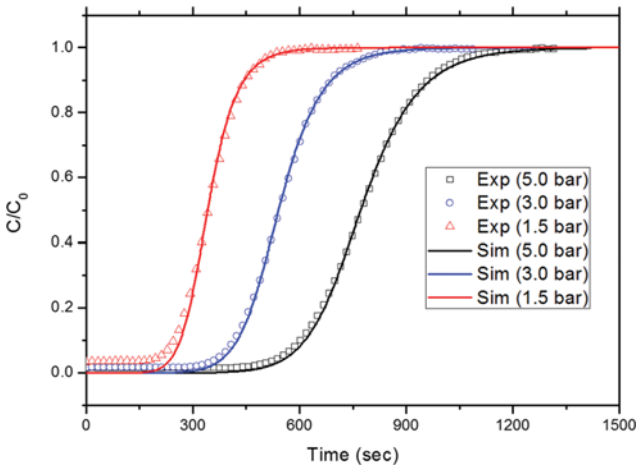

Fig. 6. CO_2 breakthrough curve at T=30 °C with Langmuir model with 2 : 1 mixture adsorption. Where, overall mass transfer coefficients for each cases are, k_{CO_2}=0.0357 s^{-1} for 5 bar, k_{CO_2}= 0.0645 s^{-1} for 3 bar and k_{CO_2}=0.1125 s^{-1} for 1.5 bar, respectively.

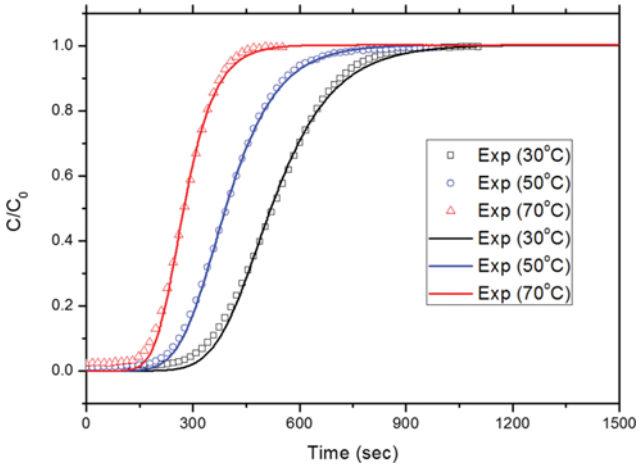

Fig. 7. CO_2 breakthrough curve at P=5 bar with Toth model with 4 : 1 mixture adsorption. Where, overall mass transfer coefficients for each cases are, k_{CO_2}=0.0282 s^{-1} for 30 °C, k_{CO_2}= 0.0345 s^{-1} for 50 °C and k_{CO_2}=0.0785 s^{-1} for 70 °C, respectively.

0.0950), L-F (SSE=0.1127) and Sips (SSE=0.1190). However, Δt for the Langmuir isotherm model is double of that for the other isotherm models, meaning that the Langmuir model cannot properly describe the amount of adsorption at equilibrium as shown in Figs. 4 and 5, which propagates the error in the breakthrough curve of Fig. 8.

The estimated constant mass transfer coefficients are shown in Tables 8 and 9 as determined by minimizing both Δt and SSE. However, the validity of the isotherm model should be evaluated with the predictive MTC model for the application of PSA and TSA process design since the mass transfer coefficient is a function of various parameters such as temperature and pressure. For this, the pressure-dependent Arrhenius form model (Eq. (17)) and the Gleuckauf's approximation (Eq. (18)) prediction model were adopted [18], and the accuracy of each model was evaluated by the SSE. The parameters and SSE of both Arrhenius form MTC and modified Gleuckauf's approximation with each isotherm model are presented in Tables 10 and 11.

$$k_i = \frac{k_{i0}}{p}\exp\left(-\frac{E_a}{RT}\right) \tag{17}$$

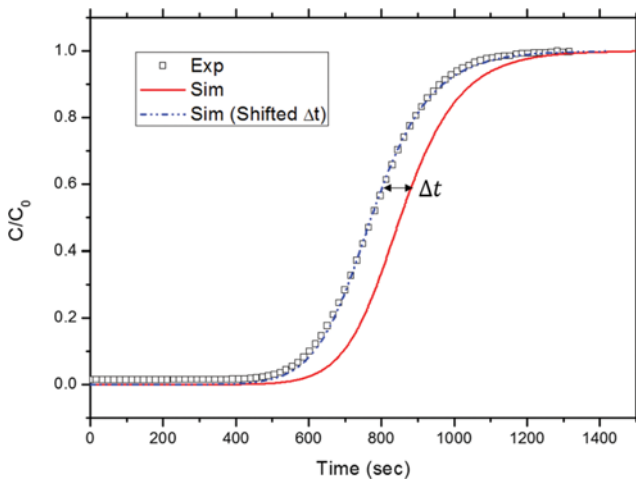

Fig. 8. CO_2 breakthrough simulation with raw experimental result and Δt considered experimental result at T=30 °C, p=5 bar with 2 : 1 mixture gas adsorption (Langmuir model).

Table 10. Parameters for pressure dependent Arrhenius mass transfer coefficient

	Langmuir	L-F	Sips	Toth	Unit
k_{i0}	1230502	2575.8	3751.7	12790.2	bar/s
E_a	41.405	26.561	27.501	30.541	kJ/mol
SSE	0.5770	0.8905	0.7442	0.6053	

Table 11. Parameters for modified Gleuckauf's approximation mass transfer coefficient

	Langmuir	L-F	Sips	Toth	Unit
τ_p	10.4	16.7	16.3	15.1	-
SSE	0.3041	0.4654	0.3183	0.2653	-

$$k_i = \frac{15 D_m \varepsilon_p c_{i0}}{r_p^2 \tau_p q_i^*} \tag{18}$$

where D_m is bulk diffusivity and τ_p is tortuosity of adsorbent particle.

The modified Gleuckauf's approximation model has less error than the Arrhenius model as confirmed in Tables 10 and 11. The MTC was inversely proportional to the pressure as shown in Tables 9 and 10. However, it was not inversely proportional to pressure as in the pressure-dependent Arrhenius form (Eq. (17)). For the Gleuckauf's approximation model in (Eq. (18)), the bulk diffusivity (D_m) is inversely proportional to pressure, but c_{i0}/q_i^* is proportional to pressure. Therefore, the modified Gleuckauf's approximation model can more precisely simulate MTC changes with respect to pressure changes than the Arrhenius model. Differing from the result of constant MTCs in Tables 8 and 9, the other three isotherm models showed much better result than that of Langmuir in Tables 10 and 11; especially, the Toth isotherm model is the most precise model when using the pressure-depen-

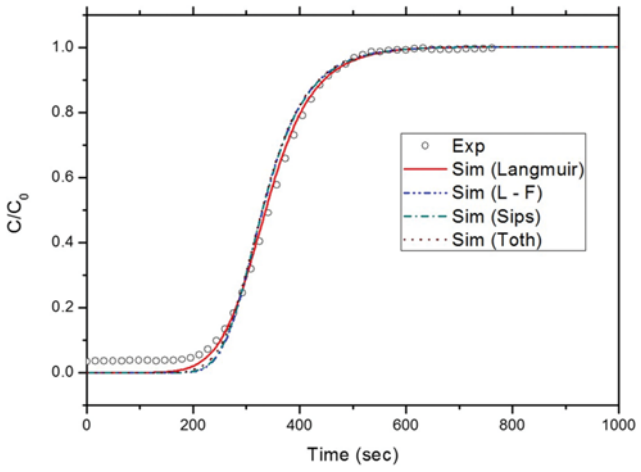

Fig. 9. CO_2 breakthrough curve at T=30 °C, p=1.5 bar, 2 : 1 mixture adsorption with pressure-dependent Arrhenius mass transfer coefficient.

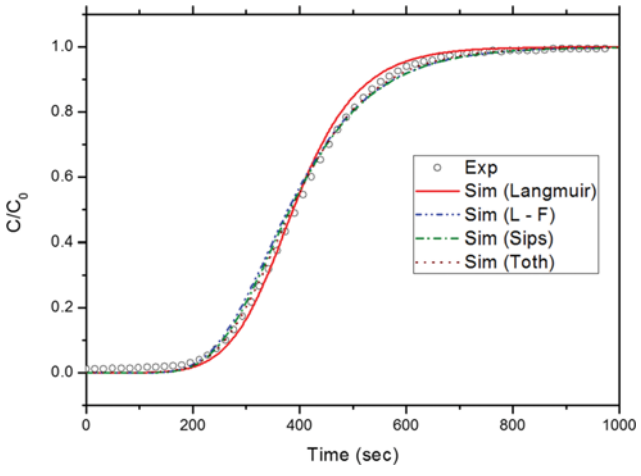

Fig. 10. CO_2 breakthrough curve at T=50 °C, p=5 bar, 4 : 1 mixture adsorption with pressure-dependent Arrhenius mass transfer coefficient.

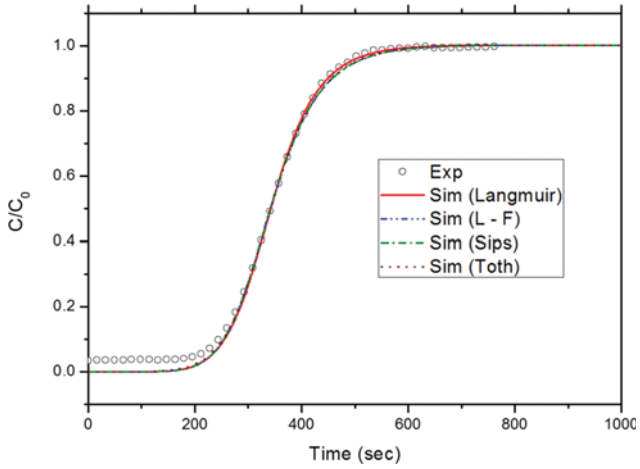

Fig. 11. CO_2 breakthrough curve at T=30 °C, p=1.5 bar, 2 : 1 mixture adsorption with modified Gleuckauf's approximation form of mass transfer coefficient.

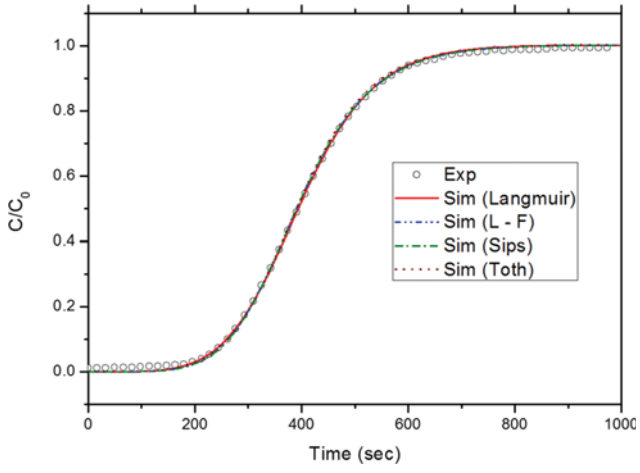

Fig. 12. CO_2 breakthrough curve at T=50 °C, p=5.0 bar, 4 : 1 mixture adsorption with modified Gleuckauf's approximation form of mass transfer coefficient.

dent MTC model.

When it comes to the result of using the pressure-dependent Arrhenius MTC model, the accuracy of the simulation result was less precise than that of constant MTCs and modified Gleuckauf's approximation model. Langmuir (SSE=0.5770) shows the best result, followed by Toth (SSE=0.6053), Sips (SSE=0.7442) and L-F (SSE=0.8905) in Table 11. Figs. 9 and 10 showed the experimental data and the simulation result using the Arrhenius model, while Figs. 11 and 12 showed those of Gleuckauf's MTC model, and Fig. 13 shows the comparison between constant MTC model, Arrhenius MTC model and modified Gleuckauf approximation MTC model. When adopting the modified Gleuckauf's approximation MTC model, the breakthrough dynamics with the Toth isotherm model showed the best result. Therefore, the Toth isotherm model described the breakthrough adsorption dynamic best of all the isotherm models for the real situation where the pressure varies in the fixed bed.

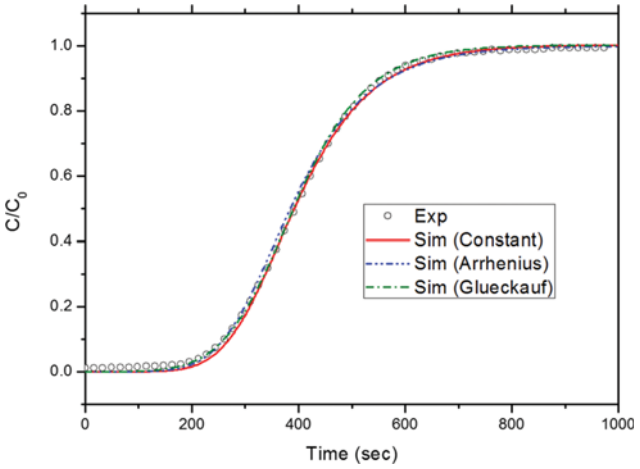

Fig. 13. CO_2 breakthrough curve at T=50 °C, p=5.0 bar, 4 : 1 mixture adsorption with constant MTC model, Arrhenius MTC model and modified Gleuckauf's approximation model (Toth isotherm).

CONCLUSIONS

We evaluated isotherm models for best describing both equilibrium adsorption capacity and breakthrough adsorption dynamics using BET and fixed-bed experiments with dynamic simulations. The model parameters of Langmuir, Langmuir-Freundlich, Sips, and Toth were determined by experimental data of pure component adsorption, and the precision of each was evaluated by SSE. The most accurate isotherm model for describing adsorption equilibrium of pure CO_2 on AC was the Langmuir-Freundlich model. For pure N_2 adsorption, the Langmuir model was the most predictive model, but accuracies of all four models were almost identical. In the breakthrough experiments with binary gas mixtures of N_2 and CO_2, the most accurate isotherm model for predicting adsorption equilibrium and transient adsorption behaviors was the Toth model. This finding suggests that the Toth isotherm model is the best choice for designing a PSA or TSA process with the coverage of adsorption equilibrium and adsorption kinetics in the corresponding research area.

ACKNOWLEDGEMENTS

The authors are grateful for the financial support from both Korea CCS R & D Center and Mid-career Researcher Program through NRF grants (NRF-2014M1A8A1049297 and NRF-2017R1A2B4008586) funded by the Ministry of Science, ICT, and Future Planning.

NOMENCLATURE

a_p : specific particle surface [m^{-1}]
C_i : molar concentration of component i [$mol \cdot m^{-3}$]
C_{i0} : feed molar concentration of component i [$mol \cdot m^{-3}$]
C_{ib} : molar concentration of component i at bed [$mol \cdot m^{-3}$]
C_{ps} : specific heat of solid adsorbent [$kJ \cdot kg^{-1}K^{-1}$]
C_{vg} : specific heat of gas [$kJ \cdot mol^{-1}K^{-1}$]

D_e : effective molar diffusivity [$m^2 \cdot s^{-1}$]
D_p : diameter of packed particle [m]
D_B : diameter of packed column [m]
F : feed molar flowrate [$mol \cdot s^{-1}$]
ΔH_i : heat of adsorption of component i [$kJ \cdot mol^{-1}$]
ΔH : heat of adsorption [$kJ \cdot mol^{-1}$]
H_s : heat transfer coefficient between gas and solid [$W \cdot m^{-2} K^{-1}$]
H_I : heat transfer coefficient between gas and column wall [$W \cdot m^{-2} K^{-1}$]
J_i : mass transfer rate of constant i [$mol \cdot m^{-3} s^{-1}$]
k_i : overall mass transfer coefficient [s^{-1}]
p : pressure [bar]
p_i : partial pressure of component i [bar]
R : gas constant [$J \cdot mol^{-1} K^{-1}$]
r_p : particle radius [m]
T : temperature [K]
T_g : gas temperature [K]
T_s : solid temperature [K]
T_w : column wall temperature [K]
u_g : gas velocity [m/s]
q_i^* : equilibrium adsorption amount of component i [$mol \cdot kg^{-1}$]
q_i : adsorption amount of component i [$mol \cdot kg^{-1}$]
w_b : bed weight [kg]
y_i : mole fraction of component i [-]
z : axial position of adsorption bed from entrance [m]

Greek Letters

ε_b : overall porosity of adsorption bed [-]
ρ_B : overall density of adsorption bed [$kg \cdot m^{-3}$]
μ : viscosity of gas phase [$kg \cdot m^{-1} s^{-1}$]
ρ_g : density of gas phase [$mol \cdot m^{-3}$]
ρ_s : density of solid [$kg \cdot m^{-3}$]
τ : relative time [sec]

SUPPORTING INFORMATION

Additional information as noted in the text. This information is available via the Internet at http://www.springer.com/chemistry/journal/11814.

REFERENCES

1. U.S. Environmental Protection Agency (EPA), Inventory of U.S. Greenhouse Gas Emissions and Sinks: 1990-2013. *U.S. EPA*, 2015.
2. J. D. Figueroa, T. Fout, S. Plasynski, H. McIlyried and R. D. Srivastava, *Int. J. Greenhouse Gas Control*, **2**, 9 (2008).
3. P. Folger, Carbon Capture: A Technology Assessment, *CRS Report for Congress* (2010).
4. C.-H. Yu, C.-H. Huang and C.-S. Tan, *Aerosol Air Quality Res.*, **12**, 745 (2012).
5. J. H. Choi, Y. E. Kim, S. C. Nam, S. H. Yun, Y. I. Yoon and J.-H. Lee, *Korean J. Chem. Eng.*, **33**, 3222 (2016).
6. J. Zhang, P. Yedlapalli and J. W. Lee, *Chem. Eng. Sci.*, **64**, 4732 (2009).
7. J. Zhang and J. W. Lee, *Ind. Eng. Chem. Res.*, **48**, 5934 (2009).
8. S. Lee, L. Liang, D. Riestenberg, O. R. West, C. Tsouris and E. Adams, *Environ. Sci. Technol.*, **37**, 3701 (2003).
9. D. M. D'Alessandro, B. Smit and J. R. Long, *Angew. Chem. Int. Ed.*, **49**, 6058 (2010).
10. S. Khalili, B. Khoshandam and M. Jahanshahi, *Korean J. Chem. Eng.*, **33**, 2943 (2016).
11. K. T. Chue, J. N. Kim, Y. J. Yoo, S. H. Cho and R. T. Yang, *Ind. Eng. Chem. Res.*, **34**, 591 (1995).
12. S. Himeno, T. Komatsu and S. Fujita, *J. Chem. Eng. Data*, **50**, 369 (2005).
13. Y.-J. Wu, Y. Yang, X.-M. Kong, P. Li, J.-G. Yu, A. M. Ribeiro and A. E. Rodrigues, *J. Chem. Eng. Data*, **60**, 2684 (2015).
14. S. Cavenati, C. A. Grande and A. E. Rodrigues, *J. Chem. Eng. Data*, **49**, 1095 (2004).
15. T. E. Rufford, G. C. Y. Watson, T. L. Saleman, P. S. Hofman, N. K. Jensen and E. F. May, *Ind. Eng. Chem. Res.*, **52**, 14270 (2013).
16. N. A. Rashidi, S. Yusup and B. H. Hameed, *Energy*, **61**, 440 (2013).
17. T. L. P. Dantas, F. M. T. Luna, I. J. Silva Jr., A. E. B. Torres, D. C. S. de Azevedo, A. E. Rodrigues and R. F. P. M. Moreira, *Brazilian J. Chem. Eng.*, **28**, 533 (2011).
18. E. Gleuckauf, *Trans. Faraday Soc.*, **51**, 1540 (1955).
19. A. Malek and S. Farooq, *AIChE J.*, **42**, 761 (1997).
20. J. Park and J. W. Lee, *Korean J. Chem. Eng.*, **33**, 438 (2016).
21. N. Casas, J. Schell, R. Pini and M. Mazzotti, *Adsorption*, **18**, 143 (2012).
22. J. Park, R. H. Kang and J. W. Lee, *Korean J. Chem. Eng.*, **34**, 1763 (2017).
23. S. H. Kang, B. M. Jeong, H. W. Choi, E. S. Ahn, S. C. Jang, S. H. Kim, B. K. Lee and D. K. Choi, *Korean Chem. Eng. Res.*, **43**, 728 (2005).
24. R. B. Bird, W. E. Stewart and E. N. Lightfoot, Transport Phenomena 2nd Ed. Wiley (2007).
25. J. M. Becnel, C. E. Holland, J. McIntyre, M. A. Matthews and J. A. Ritter, Fundamentals of Fixed Bed Adsorption Processes: Analysis of Adsorption Breakthrough and Desorption Elution Curves, *Proceedings of the 2002 American Society for Engineering Education Annual Conference & Exposition*, 2002, Session (1613).
26. Y. S. Ho, J. F. Porter and G. Mckay, *Water, Air and Soil Pollution*, **141**, 1 (2002).
27. J. W. Lee, Y. C. Ko, Y. K. Jung, K. S. Lee and Y. S. Yoon, *Comp. Chem. Eng.*, **21**, S1105 (1997).

Supporting Information

Evaluating isotherm models for the prediction of flue gas adsorption equilibrium and dynamics

Rai Hyoung Kang, Jehun Park, Dohyung Kang, and Jae W. Lee[†]

Department of Chemical and Biomolecular Engineering, Korea Advanced Institute of Science and Technology (KAIST), 291 Daehak-ro, Yuseong-gu, Daejeon 34141, Korea

(*Received 28 August 2017 • accepted 26 December 2017*)

Table S1. Uptake amount of pure N_2 on AC-RB3

Unit: p [bar], q [mol/kg]

T[a]=30 °C		T=50 °C		T=70 °C	
p_{N_2}[b]	q_{N_2}	p_{N_2}	q_{N_2}	p_{N_2}	q_{N_2}
0.033012	0.006867	0.033032	0.003479	0.033371	0.001948
0.078895	0.016243	0.079245	0.009155	0.079511	0.005672
0.113011	0.023444	0.11314	0.013669	0.113348	0.008499
0.153408	0.031246	0.153481	0.018689	0.15341	0.011289
0.19278	0.038556	0.192707	0.023497	0.192723	0.014057
0.232835	0.046014	0.232742	0.028477	0.232633	0.016916
0.273117	0.054172	0.272918	0.034351	0.272844	0.019907
0.313186	0.061249	0.313204	0.038568	0.313105	0.022459
0.353111	0.068957	0.351819	0.04328	0.351908	0.02562
0.392022	0.076876	0.393264	0.049507	0.393185	0.028905
0.433319	0.085899	0.432264	0.055246	0.432011	0.033234
0.473325	0.093427	0.471963	0.061209	0.473197	0.037103
0.511841	0.101096	0.512191	0.065894	0.512077	0.041513
0.552803	0.109875	0.552704	0.070416	0.553325	0.043465
0.592894	0.11808	0.592687	0.076119	0.611485	0.0485
0.633236	0.124803	0.632969	0.079536	0.63293	0.049845
0.67238	0.133221	0.672521	0.083919	0.672979	0.053229
0.713002	0.139786	0.712369	0.08896	0.71289	0.058091
0.752447	0.147146	0.752839	0.096011	0.752544	0.064186
0.792459	0.154078	0.793105	0.102809	0.792946	0.067134
0.832084	0.162295	0.832852	0.109805	0.851135	0.073183
0.872803	0.169086	0.873076	0.116756	0.872556	0.073954
0.912013	0.175726	0.912095	0.123442	0.931465	0.079842
0.952959	0.182432	0.952403	0.128301	0.951783	0.083377
0.991737	0.189087	0.991776	0.132706	0.992506	0.085279
1.031737	0.195152	1.032057	0.137939	1.051317	0.092727
1.072186	0.200275	1.072155	0.140307	1.072343	0.093639
1.112066	0.208356	1.13103	0.147343	1.112069	0.098224
1.132031	0.211605	1.132185	0.151916	1.132094	0.099404
1.513	0.291915	1.513	0.202315	1.513	0.167364
3.013	0.617334	3.013	0.493895	3.013	0.38844
5.013	1.002948	5.013	0.821436	5.013	0.674179

[a]Temperature uncertainty, u(T): 0.05 °C

[b]Pressure uncertainty, u(p): 1.5 kPa

Table S2. Uptake amount of pure CO_2 on AC-RB3

Unit: p [bar], q [mol/kg]

T[a]=30 °C		T=50 °C		T=70 °C	
p_{CO_2}[b]	q_{CO_2}	p_{CO_2}	q_{CO_2}	p_{CO_2}	q_{CO_2}
0.03314	0.109384	0.03325	0.065539	0.03257	0.033582
0.07652	0.215482	0.07762	0.138642	0.07862	0.078802
0.11257	0.291308	0.11266	0.189936	0.11319	0.109136
0.15268	0.3667	0.15283	0.240548	0.15281	0.139516
0.19291	0.43497	0.19289	0.289556	0.19282	0.171516
0.23274	0.496442	0.23301	0.333838	0.23316	0.200174
0.27289	0.554302	0.27289	0.376669	0.27299	0.227062
0.31271	0.608883	0.31309	0.418588	0.3128	0.256586
0.35292	0.661235	0.35293	0.457072	0.35312	0.283433
0.39258	0.712648	0.39292	0.496865	0.39187	0.307821
0.43224	0.759951	0.4325	0.534832	0.43286	0.333213
0.47221	0.805539	0.47229	0.568636	0.47223	0.362127
0.51241	0.850654	0.51274	0.603972	0.51242	0.392829
0.55244	0.897244	0.55211	0.636435	0.55249	0.419422
0.59233	0.941699	0.59188	0.666693	0.59262	0.43731
0.63225	0.985964	0.63261	0.697423	0.6317	0.458677
0.67236	1.031943	0.67244	0.729362	0.67298	0.47725
0.71263	1.073173	0.7126	0.760234	0.71182	0.505399
0.7524	1.111573	0.75184	0.788244	0.7523	0.534496
0.79221	1.148585	0.79192	0.81738	0.79213	0.560812
0.83226	1.188652	0.83209	0.846743	0.83267	0.582889
0.87233	1.225768	0.87273	0.876308	0.87211	0.601281
0.9121	1.268841	0.91274	0.908567	0.91191	0.62325
0.95242	1.301173	0.9524	0.941482	0.95237	0.639948
0.99144	1.334125	0.99236	0.975673	0.99193	0.669707
1.03207	1.374685	1.03233	1.007645	1.03243	0.697626
1.07242	1.409319	1.07217	1.036636	1.07184	0.723027
1.11138	1.445861	1.11201	1.063204	1.11218	0.741663
1.13223	1.467513	1.13186	1.074847	1.13241	0.73904
1.513	1.81006	1.513	1.311513	1.513	0.949829
3.013	2.88001	3.013	2.177735	3.013	1.638834
5.013	3.93426	5.013	2.982375	5.013	2.365212

[a]Temperature uncertainty, u(T): 0.05 °C

[b]Pressure uncertainty, u(p): 1.5 kPa